INTERNATIONAL JOURNAL OF CLIMATOLOGY
Int. J. Climatol. (2014)
Published online in Wiley Online Library
(wileyonlinelibrary.com) DOI: 10.1002/joc.3907

RMetS
Royal Meteorological Society

Short Communication

Resolving the Beaufort Sea High using synoptic climatological methods

Thomas J. Ballinger,[a]* Scott C. Sheridan[a] and Edward Hanna[b]

[a] *Department of Geography, Kent State University, OH, USA*
[b] *Department of Geography, University of Sheffield, UK*

ABSTRACT: Melt season frequencies of the Beaufort Sea High (BSH) have a profound effect on western Arctic climate, making the interannual spatial and temporal monitoring of this polar anticyclone important. This manuscript presents two automated synoptic climatological analyses using a two-step cluster procedure to classify daily mean sea level pressure (MSLP) over 180–120°W and 70–85°N with an emphasis on identifying BSH patterns. Separate raw and anomaly MSLP circulation pattern (CP) classifications are compared in order to assess the spatial characteristics of the BSH and its monthly frequency changes during the melt season from 1979 to 2012. Analysis of both classifications shows clear advantages to using the anomaly approach in terms of assessing temporal and spatial changes, particularly in light of the documented recent atmospheric circulation changes that have been observed over the region. Associations between the June anomaly circulation pattern (ACP) 5, a +4 hPa BSH pattern situated between 155°W and 135°W, and June indices of atmospheric teleconnections such as the Arctic Dipole and Arctic Oscillation are statistically significant. There is also a statistically significant link to the downstream Greenland Blocking Index; suggesting that the BSH may be intricately related to climatic variability outside the analysed domain as well. Further, ACP 5 occurred nearly 3 weeks more often during the melt season in recent massive Arctic Sea ice loss years (2007–2012) compared with the climatology (1979–2006). Recent increases in June ACP 5 frequencies account for a large proportion of this pattern's long-term frequency changes.

KEY WORDS synoptic climatology; western Arctic; circulation patterns; teleconnections

Received 16 September 2013; Revised 26 November 2013; Accepted 2 December 2013

1. Introduction

The Beaufort Sea High (BSH) plays an important role in modulating lower troposphere temperatures and sea ice variability over the western Arctic during the melt season (Drobot and Maslanik, 2003; Ballinger and Rogers, 2013). This semi-permanent pressure feature is apparent in the annual, spring, and summer pressure fields over the region and is linked to various atmospheric teleconnections that affect large-scale Arctic climate (Serreze and Barrett, 2011; Overland *et al.*, 2012). When the BSH is stronger, local temperatures are higher and less sea ice is found in the Beaufort Sea during summer (Rogers, 1978) due to increased shortwave radiation as well as coincident thermodynamic and dynamic factors that promote warm air advection, thereby enhancing melt and driving the movement of sea ice away from the coastline. Persistence of the BSH during summer 2007 fueled clear skies and warm, southerly winds which provided an ideal synoptic setting for the massive melt of sea ice in the western Arctic that greatly contributed to record basin-wide loss by the end of that summer (Stroeve *et al.*, 2008).

Composites of seasonal mean lower tropospheric circulation fields are often produced to evaluate anomalies in regional synoptic circulation features, such as the BSH. Summer (June–September; JJAS) winds at the 925 hPa level from 2007 to 2011, relative to 1979 to 2006, are shown to be more anticyclonic over the western Arctic (Ogi and Wallace, 2012). Ogi and Rigor (2013) note a mid-1990s summer (JJAS) wind shift in the region at the same atmospheric level from a cyclonic (1979–1996) to an anticyclonic (1996–2010) direction paralleling the start of the large decline in pan-Arctic sea ice. Aside from a drastic change in the mean low-level wind direction, there is also evidence in the mean sea level pressure (MSLP) fields that the core magnitude of the summer (JJA) BSH has significantly strengthened since the late 1990s (Moore, 2012).

While composite fields assess general BSH circulation characteristics, one main shortcoming of seasonal aggregation is that it provides little insight regarding day-to-day atmospheric flow variability across the western Arctic Ocean. The circulation pattern (CP) classification approach affiliated with the synoptic climatological

* Correspondence to: T. J. Ballinger, Department of Geography, Kent State University, Kent, OH 44242, USA. E-mail: tballin1@kent.edu

methodology affords researchers the opportunity to partition a specified atmospheric level into a range of CPs that are potentially related to surface conditions (Yarnal, 1993). In a recent study, Ballinger and Sheridan (2014) classified 15 raw MSLP patterns over the western Arctic and resolved a BSH pattern which occurred on roughly 30% of June days during 1979–2006, but then occurred on more than 50% of June days from 2007 to 2011 in conjunction with massive western and pan-Arctic sea ice extent losses. A few manuscripts have also resolved BSH patterns via CP classifications based on either raw or spatial anomaly data and assessed the impacts of the anticyclone on local temperature and winds (Cassano *et al.*, 2006, 2011) and sea ice motion (Asplin *et al.*, 2009) over the western Arctic. However, to the authors' knowledge no study has strictly examined melt season atmospheric circulation over the western Arctic via two distinct CP classifications comprised of raw and spatial anomaly data. In this article, comparisons are made between both approaches before the best option is identified, assessed with respect to large-scale Arctic climate variability, and examined in terms of temporal trends occurring during specified melt season months.

2. Data and methodology

2.1. Data

Daily MSLP is from the National Center for Environmental Prediction and National Center for Atmospheric Research (NCEP/NCAR) first generation reanalysis (Kalnay *et al.*, 1996), available at the NOAA/ESRL Physical Sciences Division. NCEP/NCAR reanalysis is selected because its lower tropospheric circulation fields closely follow observations and compare favourably with other reanalysis products in the western Arctic (Bromwich and Wang, 2005; Moore, 2012). Moreover, this reanalysis product has been shown to adequately depict circulation features in recent BSH-specific studies (Serreze and Barrett, 2011; Moore, 2012). The temporal focus is on the melt season, and therefore only the months between the climatological Arctic sea ice maximum (March) and minimum (September) are selected for each year between 1979–2012, resulting in 7276 classified days over the 7-month period. The gridded MSLP data are analysed at their native 2.5° latitude by 2.5° longitude horizontal resolution. The domain is 180–120°W and 70–85°N, equaling 175 total grid points, which includes most of the Beaufort and Chukchi Seas. This domain was selected to resolve the BSH based on the Serreze and Barrett (2011) climatological spring and summer BSH plots which roughly show this anticyclone centred over 150°W.

Three monthly teleconnections/climatic indices representing aspects of Arctic climate variability, the Arctic Oscillation (AO; Thompson and Wallace, 1998), Arctic Dipole (AD; Wang *et al.*, 2009; Overland and Wang, 2010), and Greenland Blocking Index (GBI; Fang 2004; Hanna *et al.*, 2013, 2014) are also compared with the resolved BSH patterns. The AO data are obtained from the Climate Prediction Center and represent the primary Empirical Orthogonal Function (EOF) of monthly 1000 hPa geopotential height anomalies from 20–90°N. The AD data are acquired from James Overland and Muyin Wang and are defined as the second EOF of anomalous extended winter (NDJFM) MSLP poleward of 70°N extrapolated for all months of the year. The Greenland Blocking Index (GBI) data, developed by Edward Hanna, are constructed from the mean 500 hPa geopotential heights over Greenland from 80–20°W and 60–80°N.

2.2. Methodology

Separate classifications are conducted using daily raw and spatial anomalies of the MSLP data. Synoptic climatological research using raw values often aims to classify the mean magnitude of common CPs (Ballinger and Sheridan, 2014), while spatial anomaly patterns are often preferred to depict the pressure gradients which determine lower-tropospheric circulation (Cassano *et al.*, 2011). The daily spatial anomalies are found by subtracting the domain mean for each day from each gridpoint in the domain. The synoptic CP classification is then carried out using SPSS Statistics Version 19.0 by subjecting each of the two datasets independently to an unrotated S-mode principal component analysis (PCA), which eliminates multicollinearity among the gridded values and reduces its dimensionality into a simpler form that explains most of the original dataset variance (Wilks, 2011). The retained principal components are then entered into an automated two-step cluster (TSC) analysis which classifies each day as a particular CP. As described by Coleman and Rogers (2007), the initial step in the TSC procedure involves classifying the first day's data field (1 March 1979) as CP 1, while the second step involves a hierarchical clustering technique whose algorithm either places the data from the subsequent day into the initial CP or creates a new CP. The process is iterated until all days are classified into a pattern which most similarly represents the data's original spatial orientation. It is important to note that one primary objective of synoptic climatology is to minimize within cluster variability while maximizing variability between clusters (Yarnal, 1993) and therefore each cluster, though composited from numerous similar daily synoptic patterns, is unique from the other classified CPs.

PCA of the raw MSLP data yields six principal components (PCs), based on eigenvalues greater than or equal to 1.0, which accounts for 98.4% of the original dataset variance. Prior to running the TSC, the log-likelihood distance measure and Bayesian information clustering criterion are selected. The PCs are then entered into the TSC procedure and seven raw circulation patterns (RCPs) based on the raw MSLP data are automatically generated. Similarly, the MSLP anomaly data produces eight PCs that explain 98.2% of the anomaly field variance. The resulting TSC of the anomaly dataset creates nine anomaly circulation patterns (ACPs). BSH patterns

in the raw fields are identified by high pressure patterns $\geq$1016 hPa, while the BSH is recognized in the anomaly fields of $\geq$+2 hPa distinct pressure cells, following the Serreze and Barrett (2011) MSLP analyses of raw and anomaly fields for overlapping melt season months. Statistical methods for analysing the BSH patterns (i.e. monthly frequencies of the patterns over the study period) are incorporated within the results of the forthcoming section.

3. Results

3.1. Raw and anomaly CPs and their monthly frequencies

The RCP classification is shown in Figure 1 and its corresponding monthly frequencies are listed at the top of Table 1. In at least four of these patterns the BSH may be identified. RCP 2, most commonly occurring during June and July (23%), shows a partially resolved BSH located over the southeastern Beaufort Sea with meridional flow apparent by the roughly north–south isobar orientation across the domain. RCP 3 exhibits broad high pressure across the domain with a small, yet strong (approximately 1028 hPa) closed high over the eastern Chukchi Sea that is early melt season (March–May) dominant. RCP 4 shows a BSH in the northeastern corner of the domain that occurs slightly more during April and May (20% and 19% respectively) than other melt season months. RCP 6 is a broad BSH pattern and is projected in the centre of the domain; however, its occurrence is roughly balanced throughout the seven melt season months, making it a common western Arctic synoptic feature.

Table 1. Mean monthly frequencies of raw (RCP) and anomaly (ACP) circulation patterns by melt season month for 1979–2012 in percent (%) of classified days.

CP	March	April	May	June	July	August	September
RCP 1	15	9	8	15	17	17	18
RCP 2	6	7	12	23	23	18	11
RCP 3	28	27	23	8	5	3	6
RCP 4	13	20	19	13	9	11	15
RCP 5	12	9	10	10	20	21	19
RCP 6	14	14	16	13	16	17	11
RCP 7	11	7	10	14	17	20	22
ACP 1	15	14	11	14	13	15	17
ACP 2	10	10	11	16	18	20	16
ACP 3	16	22	22	11	8	12	10
ACP 4	20	15	14	10	13	13	16
ACP 5	10	11	17	22	18	13	9
ACP 6	13	21	19	14	8	8	17
ACP 7	13	12	13	12	18	17	15
ACP 8	18	12	11	8	15	18	17
ACP 9	18	11	9	14	17	17	13

The ACP classification is presented in Figure 2 and its frequencies are found at the bottom of Table 1. ACPs 2, 5, 6, and 7 have positive pressure anomalies focused in the central/eastern portion of the domain, while ACPs 1, 3, and 4 are more focused on the western/central portion of the Chukchi Sea. Notably ACP 5, in which the BSH (+4 hPa) is entirely resolved in the domain, occurs most frequently during June (22%). ACPs 3 and 6, which have different geographic orientation (northwestern *versus* northeastern Beaufort Sea), are

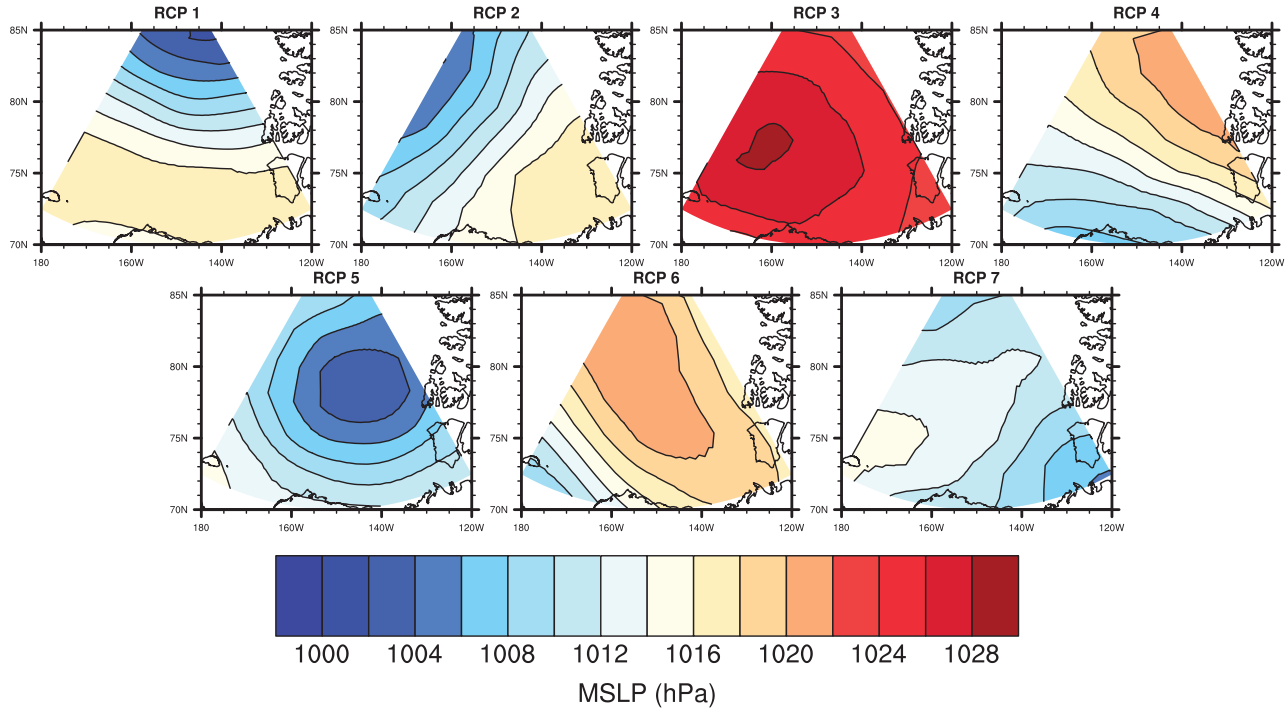

Figure 1. Raw MSLP circulation patterns (RCP) resolved by TSC procedure for the western Arctic domain.

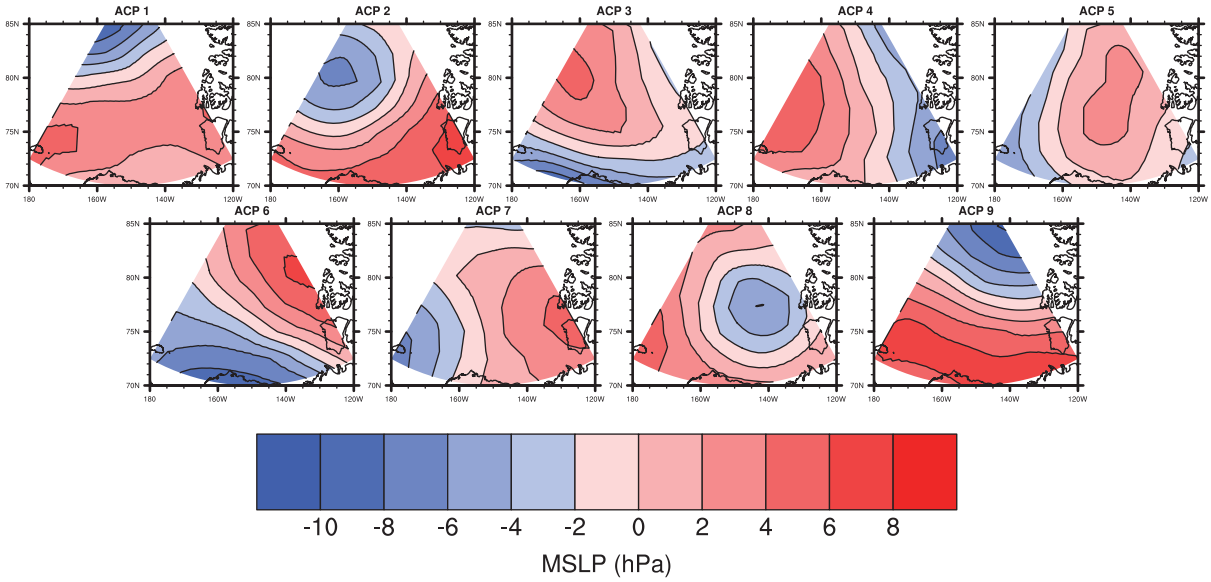

Figure 2. Anomaly MSLP circulation patterns (ACP) resolved by TSC procedure for the western Arctic domain.

most common during April and May, occurring on ≥40% of days in those months combined.

3.2. Classification comparisons

Despite a similar initial MSLP dataset, time period, and domain, the raw and anomaly patterns clearly show differences in the respective CPs. A larger number of CPs are created in the ACP catalogue than the RCP catalogue, allowing for the potential for more BSH patterns to be identified in the former classification. This difference in the number of classified patterns may be due to the fact that the TSC algorithm was not limited in the number of automated CPs it could generate or simply that the anomalies produce a greater number of variable synoptic CPs.

While some patterns are more common in certain months, there is no monthly occurrence of a particular pattern in either CP classification set that is overwhelmingly dominant relative to all others (Table 1). RCP 3 occurs 28% of the time during March, the greatest monthly frequency in either classification. In contrast, no single pattern occurs less than 3% of days in any melt season month indicating that the CPs represent the range of typical daily MSLP patterns due to the fact that at least one day per month falls under each classified pattern. Arguably the two clearest examples of BSH in both classifications, RCP 3 and ACP 5, tend to occur in different months with the former occurring more often in the early melt season, while the latter pattern occurs more during the middle of the season and likely plays a greater role in environmental warming coincident with greater high latitude insolation. More analysis reveals that little one-to-one comparison can be made between the BSH patterns in the two disparate classifications (Table S1). For instance, ACP 5 does not occur on the majority of days with another single raw pattern, but rather is spread out between four raw patterns, occurring in tandem with RCPs 2 (31% of the time), 3 (24%), 6 (19%), and 7 (20%).

Divisions of the patterns preceding and encapsulating record Arctic sea ice minima [1979–2006 (hereafter, *climatology*) and 2007–2012 (hereafter, *recent*)] show clear melt season frequency differences between the classifications (Table 2 and Table S2). While the frequencies of RCPs 4 and 7 have increased nearly a week in recent years *versus* the climatology, ACP 5 has increased almost 3 weeks (approximately 20 days), offset partially by decreases in ACP 9. Increases in ACP 5, and to a lesser extent ACP 6 (approximately 4 days), show that anomaly patterns that depict the BSH are becoming more prevalent in the eastern Beaufort Sea at the expense of ACPs such as 4 and 8 that have BSH features in the western portion of the domain. Roughly following Ogi and Rigor (2013; hereafter *OR*), the 1979–1995 and 1996–2012 periods show a nearly 10-day melt season increase in ACP 5 from the former to latter periods, suggesting greater ACP frequencies in recent years may have initiated in the mid-1990s.

3.3. Relationships to teleconnection and climatic indices

Previous research has identified atmospheric circulation changes taking place in the western Arctic during June and an increased occurrence of surface and mid-tropospheric weather patterns reminiscent of the BSH (Overland *et al.*, 2012; Ballinger and Sheridan, 2014). Given the observed June BSH changes found in previous studies and in this article (see Section 3.4), it is necessary to examine how these relate to other large-scale climate variability in the Arctic. To address this question, Pearson bivariate correlations are calculated between each pattern's June frequency and the June AD, AO, and GBI

Table 2. Mean melt season frequencies of the nine anomaly circulation patterns (ACP) by different period divisions.

ACP	ACP 1	ACP 2	ACP 3	ACP 4	ACP 5	ACP 6	ACP 7	ACP 8	ACP 9
$Overall_{1979-2012}$	20.88	23.15	26.15	23.47	35.29	22.50	25.00	16.24	21.32
$OR_{1979-1995}$	19.94	25.00	27.82	25.12	30.41	20.18	24.53	16.35	24.65
$OR_{1996-2012}$	21.82	21.29	24.47	21.82	40.18	24.82	25.47	16.12	18.00
$Climatology_{1979-2006}$	21.00	23.96	26.50	24.14	31.71	21.75	25.11	16.79	23.04
$Recent_{2007-2012}$	20.33	19.33	24.50	20.33	52.00	26.00	24.50	13.67	13.33
Net (Climatology − Overall)	+0.12	+0.81	+0.35	+0.67	−3.58	−0.75	+0.11	+0.55	+1.72
Net ($OR_{1996-2012} - OR_{1979-1995}$)	+1.88	−3.71	−3.35	−3.30	**+9.77**	+4.64	+0.94	−0.23	−6.65
Net (Recent − Overall)	−0.55	−3.82	−1.65	−3.14	**+16.71**	+3.5	−0.50	−2.57	**−7.99**
Net (Recent − Climatology)	−0.67	−4.63	−2.00	−3.81	**+20.29**	+4.25	−0.61	−3.12	**−9.71**

OR references refere to Ogi and Rigor (2013) who noted a near-surface circulation shift about the year 1996. *Recent* refers to the period of six lowest Arctic sea ice summers since 1979. Net changes exceeding 1 week are bolded.

as displayed in Table 3. The RCP values (top) show only two correlation coefficients above/below ±0.30, of which only the correlation between GBI June and RCP 4 ($r = +0.35$) is significant ($p = 0.05$). On the other hand, the ACP frequencies (bottom) are very well-correlated to the indices. With the exception of the strongly zonal pattern (ACP 9), BSH ACPs 2, 5, 6, and 7 are all related to the indices with a high degree of statistical significance. June ACP 5 is especially notable, negatively correlated to AD ($r = -0.72$) and AO ($r = -0.65$) and positively to the GBI ($r = +0.72$), all at $p = 0.01$. High intercorrelation between the AO and AD June indices ($r = +0.75$, $p = 0.01$), and hence similar association with ACP 5, is not surprising since a wavier, blocking negative AO pattern lends itself to more persistent regional circulation features across the Arctic during this month (Overland *et al.*, 2012).

On the basis of Table 3, ACP 5 clearly relates best to the Arctic climatic variability over the entire period, but in order to more carefully examine interannual variability between the indices and the pattern's monthly frequency time series overplots are constructed (Figure 3). The anticorrelation between AD (top) and AO (middle) is apparent as these two indices are out-of-phase throughout the time series, especially in the mid-1990s and since 2007. The strong positive correlation with the GBI (bottom) is particularly in-phase during the early 1990s and from 2006 onward. Whereas declines in the respective AD and AO atmospheric fields correspond to a rise in the BSH frequencies, the June BSH occurrence increases mirror the amplification of the GBI's 500 hPa geopotential height fields; the latter are associated with the strong ridging witnessed over Greenland in the past several years that have facilitated large increases in ice sheet surface melt during summer (Nghiem *et al.*, 2012; Fettweis *et al.*, 2013; Hanna *et al.*, 2013, 2014; Tedesco *et al.*, 2013).

Table 3. Pearson bivariate correlations of June raw (RCP) and anomaly (ACP) frequencies *versus* the AD, AO, and GBI June indices.

CP	AD_{June}	AO_{June}	GBI_{June}
RCP 1	+0.25	+0.21	−0.23
RCP 2	+0.11	−0.01	−0.04
RCP 3	−0.11	−0.22	+0.07
RCP 4	−0.26	−0.17	*+0.35*
RCP 5	+0.22	+0.15	−0.16
RCP 6	+0.05	+0.16	−0.18
RCP 7	−0.34	−0.18	+0.25
ACP 1	+0.10	+0.26	−0.19
ACP 2	**+0.49**	**+0.58**	**−0.49**
ACP 3	−0.30	−0.32	+0.16
ACP 4	+0.33	+0.18	−0.26
ACP 5	**−0.72**	**−0.65**	**+0.72**
ACP 6	**−0.51**	**−0.53**	**+0.52**
ACP 7	**+0.67**	**+0.45**	*−0.43*
ACP 8	+0.05	+0.27	−0.18
ACP 9	**+0.60**	**+0.52**	**−0.60**

Significant correlations at $p = 0.05$ are italicized, while those at $p = 0.01$ are bolded.

3.4. Change analysis of ACP 5

Analysis in Section 3.2 shows melt season increases in ACP 5 frequencies in recent years, which is supported by previously mentioned studies that also suggest that June BSH frequencies are greatly changing over similar time periods. Therefore, further analysis of the BSH temporal variability is necessary to give added perspective regarding possible long-term changes. The time series of the frequencies of June ACP 5 (Figure 3) appear to be increasing over time, particularly since the mid-1990s. As a result, a simple linear trend was fitted to the monthly frequency data of ACP 5 revealing a +0.17 June days $year^{-1}$ increase that is statistically significant ($p = 0.03$). Over the 34-year study period, this change equates to a nearly 6-day increase in the BSH pattern.

Analysis of subperiods (i.e. Table 2) by June months reveals $OR_{1979-1995}$ has an insignificant −0.31 June days $year^{-1}$ trend, however the trend of $OR_{1996-2012}$ is strongly positive and statistically significant (+0.62, $p = <0.01$), which explains the overall melt season increases of the last 17 years. When the last 6 years of the entire time series is truncated, there is no statistically significant trend (≤ -0.01, $p = \geq 0.99$) suggesting that successive high ACP 5 frequencies during recent June months may be enhancing the June trend and a step-like increase in the anticyclone's occurrence. Separate *t*-tests between the frequencies of the two OR periods ($t = -2.03$, $p = 0.05$) and the climatology and recent

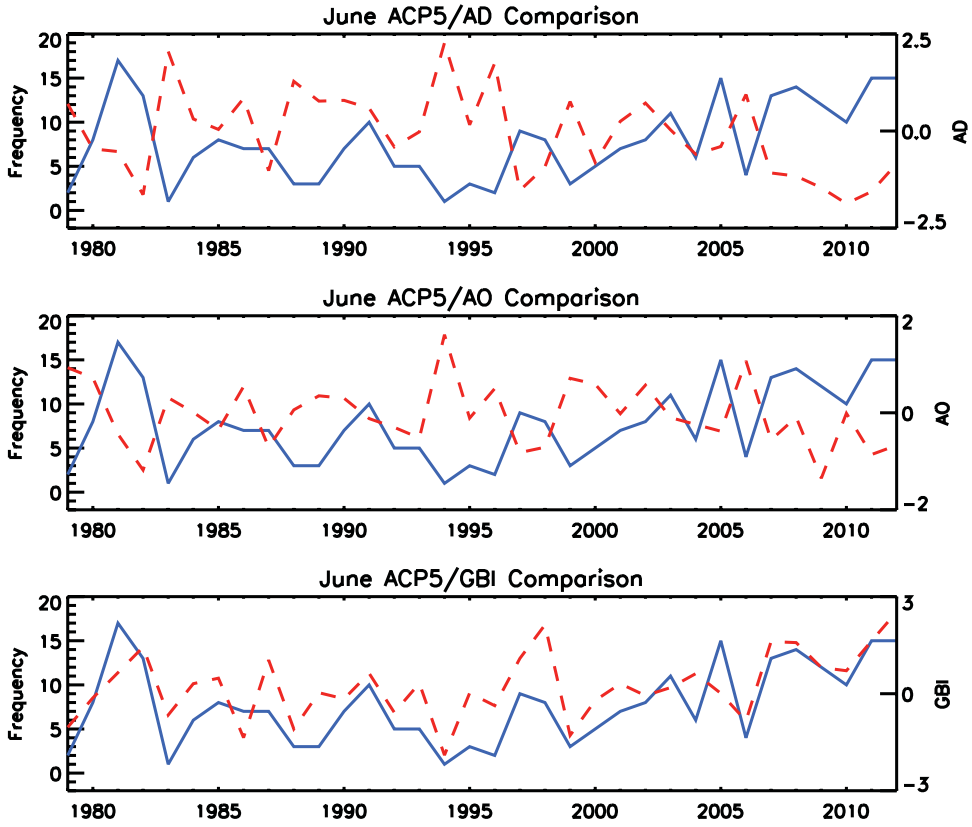

Figure 3. Time series of June ACP 5 frequencies (solid line) and AD, AO, and GBI June values (dashed line).

ACP 5 frequencies ($t = -3.88$, $p = <0.01$) confirm that the means of each of the subperiods are significantly different from each other and that the observed BSH frequency changes are statistically stronger in recent years. This closely corresponds with the increase in the GBI since the early 2000s (Hanna *et al.*, 2013).

Other summer months are also accounting for the approximately 3-week change in the ACP 5 BSH pattern. July (not shown) has a $+0.11$ days year^{-1} increase that is not significant ($p = 0.13$), while August (also not shown) has witnessed a $+0.20$ days year^{-1} increase ($p = <0.01$) that accounts for almost a 7-day increase over time. The rise in June and August pattern frequencies, in particular, represent approximately 65% of ACP 5 melt season increases since 1979 and in general, are consistent with the findings of Ballinger and Sheridan (2014) that found notable positive BSH frequency departures from the climatology during these months.

4. Discussion and conclusions

Using two different techniques for classification of MSLP data, one examining raw magnitudes and the other investigating spatial anomalies, two very different spatial and temporal results occur. Concurrent with previous synoptic climatological research by Ballinger and Sheridan (2014), classification and analysis of the raw reanalysis data shows an increase in the BSH pattern over the western Arctic, especially during high sea ice loss years. Cassano *et al.* (2011) resolve several BSH-like anomaly patterns in their synoptic classification, though the frequencies of these patterns are essentially non-existent during JJA months. These differences are likely an artefact of different synoptic methods (TSC versus self-organizing maps) and study periods among other causes. While the aforementioned synoptic climatological studies show the ability of synoptic methods to depict BSH patterns, their methodological differences makes their derived results difficult to compare.

Given a common clustering technique, it is striking that the RCP magnitudes reveal relatively little about circulation variability when compared to the magnitudes of the anomaly patterns. From the ACPs and subsequent temporal analysis, much more information can be gleaned about the resulting circulation fields and their melt season occurrence. For instance, with few exceptions, there appears to be an eastward spatial shift in BSH anomaly patterns across the domain as suggested by the remarkable frequency change over the recent period. This observed circulation change is likely aiding the western Arctic sea ice melt through poleward warm air advection off the adjacent land and diabatic heating while supporting wind-driven export of the ice cover into the Beaufort Gyre. It is also likely that this circulation change is having other cryospheric impacts through a variety of interconnected physical mechanisms suggested in this manuscript. Should the increased prevalence of BSH frequencies sustain, one would expect profound changes

in the energy budget of the region to transpire with much more sunlight entering the Beaufort and eastern Chukchi Seas as sea ice often becomes unfast from the coastline during June (Mahoney *et al.*, 2007; Galley *et al.*, 2012).

Connections to large-scale Arctic climate between the AD, AO, GBI, and ACP 5 are also strong through time. In particular, the recent strong covariance between the indices and BSH frequencies is physically supported as increased atmospheric blocking over the North American Arctic, perpetuating a BSH pattern, can be attributed to a negative AO and regionally negative AD (Overland *et al.*, 2012). Increased blocking is also clearly related to a positive GBI (Hanna *et al.*, 2013). Frequencies of strong summer blocking events across the western Arctic and Greenland appear to be related through time (Pfahl and Wernli, 2012), with the mechanism linking these events potentially due to negative phases of the AO/AD and/or Arctic amplification (Francis and Vavrus, 2012).

This manuscript shows advantages to using spatial anomalies *versus* raw MSLP patterns when conducting synoptic CP classification in this region. Though a concise domain for circulation analysis is presented, two very different sets of results are generated depending on the entry of the data, raw or anomaly, into the clustering algorithm. The benefits of the research outcomes should be of interest to both synoptic climatologists evaluating how to process MSLP data before classification *and* to polar climate researchers in search of the more robust approach to analysing near-surface atmospheric circulation variability over the Arctic Ocean via reanalysis data, especially given a limited area of study.

Acknowledgements

The authors would like to thank Mary Haley (NCAR/CISL) for assistance with the NCL script used to plot the circulation patterns and James Overland (NOAA/PMEL) and Muyin Wang (JISAO/University of Washington) for sharing the AD dataset. The authors would also like to thank the two anonymous reviewers for their insightful comments which improved this manuscript.

Supporting Information

The following supporting information is available as part of the online article:

Table S1. Pivot table of anomaly circulation pattern (ACP) frequencies by raw circulation pattern (RCP) frequencies (%).

Table S2. Mean melt season frequencies of the seven raw circulation patterns (RCP) by different period divisions. *OR* references Ogi and Rigor (2013) who noted a near-surface circulation shift about the year 1996. *Recent* refers to the period of six lowest Arctic sea ice summers since 1979. Net changes exceeding 1 week are bolded.

References

Asplin MG, Lukovich JV, Barber DG. 2009. Atmospheric forcing of the Beaufort Sea ice gyre: surface pressure climatology and sea ice motion. *J. Geophys. Res.* **114**: C00A06, DOI: 10.1029/2008JC005127.

Ballinger TJ, Rogers JC. 2013. Atmosphere and ocean impacts on recent western Arctic summer sea ice melt. *Geogr. Compass* **7**: 686–700, DOI: 10.1111/gec3.12077.

Ballinger TJ, Sheridan SC. 2014. Associations between circulation pattern frequencies and sea ice minima in the western Arctic. *Int. J. Climatol.*, DOI: 10.1002/joc.3767 (in press).

Bromwich DH, Wang S-H. 2005. Evaluation of the NCEP/NCAR and ECMWF 15/40-yr reanalyses using rawinsonde data from two independent Arctic field experiments. *Mon. Weather Rev.* **133**: 3562–3578.

Cassano EN, Lynch AH, Cassano JJ, Koslow MR. 2006. Classification of synoptic patterns in the western Arctic associated with extreme events at Barrow, Alaska, USA. *Clim. Res.* **30**: 83–97.

Cassano EN, Cassano JJ, Nolen M. 2011. Synoptic weather pattern controls on temperature in Alaska. *J. Geophys. Res.* **116**: D11108, DOI: 10.1029/2010JD015341.

Coleman JS, Rogers JC. 2007. A synoptic climatology of the central United States and associations with Pacific teleconnection pattern frequency. *J. Climate* **20**: 3485–3497.

Drobot SD, Maslanik JA. 2003. Interannual variability in summer Beaufort Sea ice conditions: relationship to winter and summer surface and atmospheric variability. *J. Geophys. Res.* **108**: 3233, DOI: 10.1029/2002JC001537.

Fang Z-F. 2004. Statistical relationship between the northern hemisphere sea ice and atmospheric circulation during wintertime. In *Observation, Theory and Modeling of Atmospheric Variability*. World Scientific Series on Meteorology of East Asia, Zhu X (ed). World Scientific Publishing Company: Singapore; 131–141.

Fettweis X, Hanna E, Lang C, Belleflamme A, Erpicum M, Gallée H. 2013. Important role of the mid-tropospheric atmospheric circulation in the recent surface melt increase over the Greenland ice sheet. *Cryosphere* **7**: 241–248.

Francis JA, Vavrus SJ. 2012. Evidence linking Arctic amplification to extreme weather in the mid-latitudes. *Geophys. Res. Lett.* **39**: L06801, DOI: 10.1029/2012GL051000.

Galley RJ, Else BGT, Lukovich JV, Howell SEL, Barber DG. 2012. Landfast sea ice conditions in the Canadian Arctic: 1983–2009. *Arctic* **65**: 133–144.

Hanna E, Jones JM, Cappelen J, Mernild SH, Wood L, Steffen K, Huybrechts P. 2013. The influence of North Atlantic atmospheric and oceanic forcing effects on 1900–2010 Greenland summer climate and ice melt/runoff. *Int. J. Climatol.* **33**: 862–880, DOI: 10.1002/joc.3475.

Hanna E, Cappelen J, Fettweis X, Mernild S, Mote T, Steffen K, Wood L. 2014. Atmospheric and oceanic forcing of the exceptional Greenland ice sheet surface melt in summer 2012. *Int. J. Climatol.*, DOI: 10.1002/joc.3743 (in press).

Kalnay E, Kanamitsu M, Kistler R, Collins W, Deaven D, Gandin L, Iredell M, Saha S, White G, Woollen J, Zhu Y, Chelliah M, Ebisuzaki W, Higgins W, Janowiak J, Mo KC, Ropelewski C, Wang J, Leetmaa A, Reynolds R, Jenne R, Joseph D. 1996. The NCEP/NCAR 40-year reanalysis project. *Bull. Am. Meteorol. Soc.* **77**: 437–471.

Mahoney A, Eikcen H, Shapiro L. 2007. How fast is landfast sea ice? A study of the attachment and detachment of nearshore ice at Barrow, Alaska. *Cold Reg. Sci. Technol.* **47**: 233–255.

Moore GWK. 2012. Decadal variability and a recent amplification of the summer Beaufort Sea High. *Geophys. Res. Lett.* **39**: L10807, DOI: 10.1029/2012GL051570.

Nghiem SV, Hall DK, Mote TL, Tedesco M, Albert MR, Keegan K, Shuman CA, DiGirolamo NE, Neumann G. 2012. The extreme melt across the Greenland ice sheet in 2012. *Geophys. Res. Lett.* **39**: L20502, DOI: 10.1029/2012GL053611.

Ogi M, Rigor IG. 2013. Trends in Arctic sea ice and the role of atmospheric circulation. *Atmos. Sci. Lett.* **14**: 97–101, DOI: 10.1002/asl2.423.

Ogi M, Wallace JM. 2012. The role of summer surface wind anomalies in summer Arctic sea ice extent in 2010 and 2011. *Geophys. Res. Lett.* **39**: L09704, DOI: 10.1029/2012GL051330.

Overland JE, Wang M. 2010. Large-scale atmospheric circulation changes are associated with the recent loss of Arctic sea ice. *Tellus A* **62**: 1–9.

Overland JE, Francis JA, Hanna E, Wang M. 2012. The recent shift in early summer Arctic atmospheric circulation. *Geophys. Res. Lett.* **39**: L19804, DOI: 10.1029/2012GL053268.

Pfahl S, Wernli H. 2012. Quantifying the relevance of atmospheric blocking for co-located temperature extremes in the Northern Hemisphere on (sub-)daily time scales. *Geophys. Res. Lett.* **39**: L12807, DOI: 10.1029/2012GL052261.

Rogers JC. 1978. Meteorological factors affecting interannual variability of summertime ice extent in the Beaufort Sea. *Mon. Weather Rev.* **106**: 890–897.

Serreze MC, Barrett AP. 2011. Characteristics of the Beaufort Sea High. *J. Climate* **24**: 159–182.

Stroeve J, Serreze M, Drobot S, Gearhead S, Holland M, Maslanik J, Meier W, Scambos T. 2008. Arctic sea ice extent plummets in 2007. *EOS: Trans. Am. Geophys. Union* **89**: 13–20.

Tedesco M, Fettweis X, Mote T, Wahr J, Alexander P, Box J, Wouters B. 2013. Evidence and analysis of 2012 Greenland records from spaceborne observations, a regional climate model and reanalysis data. *Cryosphere* **7**: 615–630.

Thompson DWJ, Wallace JM. 1998. The Arctic oscillation signature in the wintertime geopotential height and temperature fields. *Geophys. Res. Lett.* **25**: 1297–1300.

Wang J, Zhang J, Watanabe E, Ikeda M, Mizobata K, Walsh JE, Bai X, Wu B. 2009. Is the Dipole Anomaly a major driver to record lows in Arctic summer sea ice extent? *Geophys. Res. Lett.* **36**: L05706, DOI: 10.1029/2008GL036706.

Wilks DS. 2011. *Statistical Methods in the Atmospheric Sciences*, 3rd edn. Academic Press: Oxford, UK.

Yarnal B. 1993. *Synoptic Climatology in Environmental Analysis: A Primer*. Belhaven Press: London, UK.

